Computer Assisted Mechanics and Engineering Sciences, **10**: 45–56, 2003.

Three-dimensional finite element simulations of various roll's shape during three-roll planetary rolling processes

Shyue-Jian Wu, Ming-Hu Chang and Yeong-Maw Hwang
Department of Mechanical Engineering, National Sun Yat-Sen University
Kaohsiung, Taiwan 80424, Republic of China

(Received November 21, 2000)

The purpose of this paper is to analyze the bar rolling process by means of various roll's shapes under the reduction zone of a three-roll planetary mill. The problems were solved with the aid of the finite element program MARC adopting the large deformation–large strain theory and the updated Lagrangian formulation (ULF) and a mesh rezoning procedure was adopted to improve the unexpected error of element turning inside out. The mesh system of the whole bar billet was established by using three-dimensional brick elements, and the three-dimensional elastic-plastic finite element model in MARC was chosen to perform the simulation of the three-roll planetary rolling processes. Totally five different roll's shapes were used to simulate the rolling process. The numerical results; such as the equivalent von Mises stress and plastic strain distributions, rolling force, rolling moment, billet speeds at the entrance and exit planes of the roll gap, etc., are useful in the design of three-roll planetary rolling processes.

Keywords: three-roll planetary rolling process, mesh rezoning, roll's shape design

1. Introduction

A three-roll planetary mill is an effective design for a high reduction rolling process than other conventional rolling process [1]. The mechanism of a three-roll planetary mill is carried out in the following manner. The rolls are driven by a main drive planetary gear system and a superposed drive gear system as shown in Fig. 1. The main drive gear system makes the axis of the sun gear rotate around the billet. The superposed drive gear system will be driven additionally to eliminate any slight rotation of the outlet material. The axis of the roll can be adjusted to form an offset angle (α) and inclined angle (β), as shown in Figs. 2 and 1, respectively. The axes of three conical rolls are arranged at an angle of 120° in relation to one another, which rotate around the deformable bar billet. In general, the surface of rolls is composed of two parts, one is the reduction zone with a tapered cone, and the other is the smoothing zone with a smaller tapered cone and sphere fillet at the corner. The round billets are conveyed through a supporting pipe located in the center of the three-roll mill by a back pushing plate, until it can be pulled into the roll gap by the rolls, and then it is rolled out. Various cross-sectional area of the product can be easily obtained by simply adjusting the axes of the three rolls. An important advantage of the three-roll planetary mill is that during the process the operating temperature of the billet is almost under an isothermal state.

Rolling is one of the important metal forming processes in industry. And the analytical and experimental methods have been investigated for more than half a century. With the aid of the high-speed computers in recent years, the distribution of field variables in full detail becomes predictable. Li and Kobayashi [5] employed the rigid-plastic material model with the infinitesimal theory of plastic deformation to analyze the plane strain rolling. Mori and Osakada [7] used a rigid-plastic model finite element method to simulate the shape rolling in three-dimensional steady state deformation. Shiau and Kobayashi [12] employed the rigid-viscoplastic formulation to a three-dimensional finite

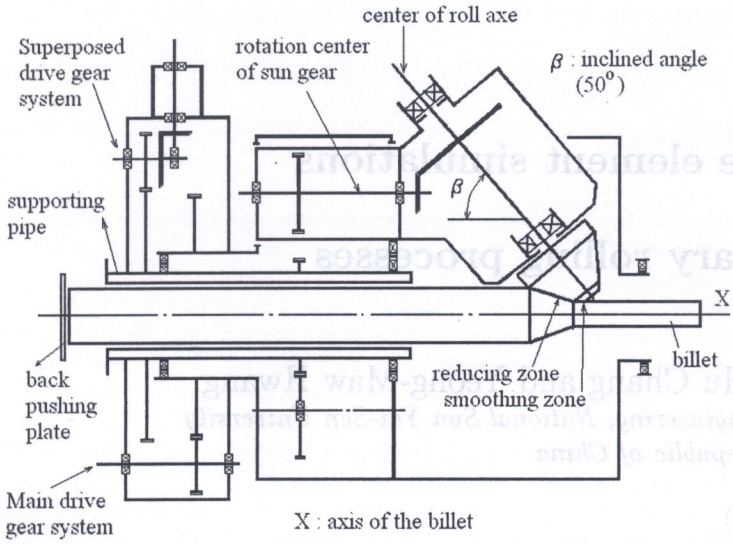

Fig. 1. Schematic diagram of the three-roll planetary mill

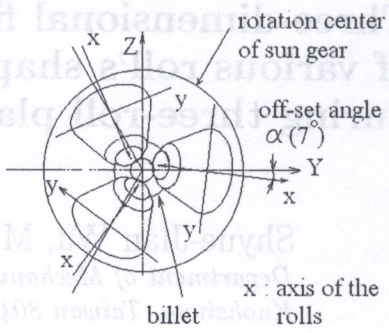

Fig. 2. End view of the three-roll planetary mill

element analysis of open die forging. Noma, et al. [9] adopted a rigid-plastic finite element method with the assumption of axis-symmetric model to simulate the three-roll planetary mill process. Aoyagi and Ohta [2] investigated the rolling force and pressure of the roll by the experiments of plasticine. But it had been very difficult to make a complete analysis for a whole simulation of the metal forming process with a three dimensional element model. When a three-dimensional element model is used to implement, it will take a large amount of computing time [10]. To simplify the analysis of the three-roll planetary rolling process, the rolls are simulated with stiff surfaces which rotate on their axis but not on the axis of the billet. As well, the front shape of the billet is conical to make the entrance easy.

The objectives of this paper are to create the elemental mesh system, then to find the initial contact position of the billet and rolls for simulation, and finally to obtain the stress and strain distribution of the billet at the roll gap. With a finite element package MARC [4, 8, 11], this research adopts three-dimensional brick elements with the elastic-plastic material model to simulate the three-roll planetary rolling process. After numerical simulations, the rolling forces, the rolling moment, and the velocities of the billet in the steady state will be discussed in this paper.

2. The elastic-plastic finite element formulation

During metal forming process, the billet undergoes large plastic deformation and rotation. It is necessary to consider geometric non-linearity, material non-linearity and constitutive non-linearity in the large strain plastic problem. Based on the Truesdell rate of Cauchy stress and the updated Lagrangian formulation, the rate of virtual work is given by the following [3, 6],

$$\int_v \left[\dot{\sigma}_{ij}^T \frac{\delta u_i}{\partial x_j} + \sigma_{ij} \frac{\partial v_k}{\partial x_i} \frac{\partial \delta u_k}{\partial x_j} \right] \mathrm{d}v = \int_v \dot{q}_i \delta u_i \, \mathrm{d}v + \int_s \dot{t}_i \delta_i \, \mathrm{d}s, \tag{1}$$

where $\dot{\sigma}_{ij}^T$ is the Truesdell rate of Cauchy stress, u_i is the displacement field of the spatial particle, x_i is the spatial position vector of a particle described as deformed coordinate configurations, v_i is the velocity field of the spatial particle, $\dot{q}_i$ is the rate of distributed load per unit volume in the deformed situation, and $\dot{t}_i$ is the rate of boundary (surface) load. The integration was carried out over the current volume and surface.

2.1. Treatment of contact and friction

The initial contact position of the problem can be computed by the means of halving the interval (bisection method). In Fig. 3, contact problem between the rigid body and deformable bar billet can be used as solver constraints in MARC. The non-penetration constraint is defined by

$$\vec{u}_A \cdot \vec{n} \leq D \tag{2}$$

where $\vec{u}_A$ is the displacement vector of node A of the deformable bar billet, and $\vec{n}$ is the unit normal vector of the rigid die, D is the distance between the rigid die and the node A of the deformable bar billet.

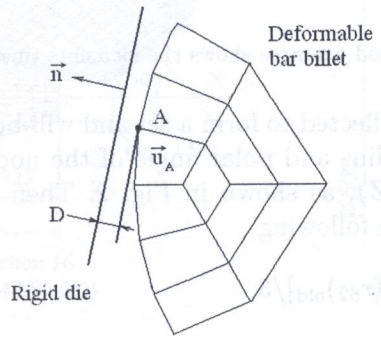

Fig. 3. Definition of contact problem

Whenever contacting between a deformable body and a rigid body is detected, imposed displacement is automatically created. A check is made on all free boundary nodes to determine whether the newly calculated displacement increments put them inside any surface. If the increment is reduced, the current increment is considered split into two and the remainders are executed next.

In this paper, Coulomb friction is used for the modeling of the interface between the billet and rolls, the formulation of which is given by the following vector form [4],

$$\vec{f}_t = -\mu f_n \frac{2}{\pi} \tan^{-1}\left(\frac{|\vec{v}_r|}{C}\right) \vec{t} \tag{3}$$

where $\vec{f}_t$ is the tangential force being applied, μ is the coefficient of friction, f_n is the normal reaction stress, $\vec{t}$ is tangential unit vector, and $\vec{v}_r$ is the relative slide velocity. The constant C smoothens more or less the step function. Typically, the magnitude of C should be one or two orders lower than the average sliding velocity in the contact region. In this paper, the constant C adopted is 0.05 mm time increment.

2.2. Treatment of rezoning

The elements of the deformable bar billet in the three-roll planetary rolling process usually undergo serious distortion, even might cause elements turning inside out. In Fig. 4, a failed simulation example shows the stage of the elements turning inside out because of the serious distortion of the nodal point. To deal with this problem, a treatment of mesh rezoning was adopted in this study [13]. In order to obtain the right outer shape of the bar billet, only its interior nodal points are rezoned. The rezoning increment is implemented by calling a self-written subroutine at every 20 usual increments, and then the corresponding field variables such as stress field, velocity field, etc., at this newly established have to be calculated.

As further shown in Fig. 8, the numbering system of elemental nodes, such as node numbers 2, 32, and 62, are symmetrical with the axis of the billet and arranged at an angle of 120° in relation

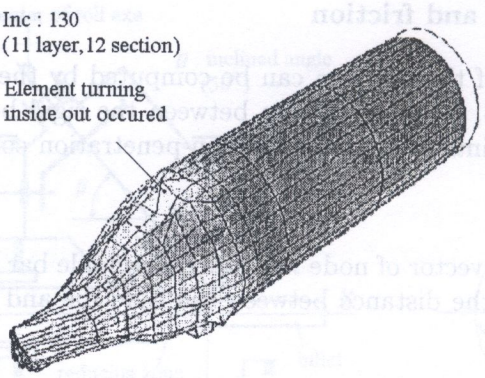

Fig. 4. A failed example shows the elements turning inside out

to one another. These nodes are collected to form a set and will be rezoned by the following method. Let (r_i) and (θ_i) stand for the radius and polar angle of the nodal point with the reference of the global coordinates system (X, Y, Z), as shown in Fig. 2. Then we have the newly defined nodal coordinates of the nodal set in the following,

$$(r_i)_{\text{new}} = [(r_2)_{\text{old}} + (r_{32})_{\text{old}} + (r_{62})_{\text{old}}]/3, \tag{4}$$

$$(\theta_i)_{\text{new}} = (\theta_i)_{\text{old}}\,, \tag{5}$$

$$(X_i)_{\text{new}} = [(X_2)_{\text{old}} + (X_{32})_{\text{old}} + (X_{62})_{\text{old}}]/3, \tag{6}$$

$$(Y_i)_{\text{new}} = (R_i)_{\text{new}} \cos(\theta_i)_{\text{new}}\,, \tag{7}$$

$$(Z_i)_{\text{new}} = (R_i)_{\text{new}} \sin(\theta_i)_{\text{new}}\,, \tag{8}$$

where subscript i stands for nodes 2, 32, and 62, subscripts 'old' and 'new' denote the variable before and after the rezoning increment. After having defined all the nodal point sets of the billet, one can computes the new defined variables by a call subroutine supported in MARC.

3. Analysis Conditions

This research adopted one deformable bar billet model and five kinds of roll's shape to simulate the rolling processes. According to the five different roll shapes, the simulation cases are named from B1 to B5. The initial contact position of the billet and the roll for case B1 is shown in Fig. 5. The main different among the roll's shape is that the reduction zone was composed of two taper cones by increasing two degrees in left side and decreasing on the right side. The dimensions of the roll for cases B1 to B5 is shown in Fig. 6 and tabulated in Table 1, respectively.

Table 1. The dimensions of the roll for cases B1 to B5

Dimension	Case B1	Case B2	Case B3	Case B4	Case B5
A	29°	31°	33°	35°	37°
B	37°	35°	33°	31°	29°
C	116.65 mm	114.09 mm	none	109.03 mm	106.49mm

The numbering system of the bar billet of the elements and nodes are shown in Figs. 7 and 8, respectively.

The simulation of the three-roll planetary mill is composed of a deformable bar billet, a back pushing plate to push the bar billet from left to right, a rigid supporting pipe to support the bar billet, and three rigid rolls to roll out the deformable bar billet. The surface of rolls is set to be a rigid

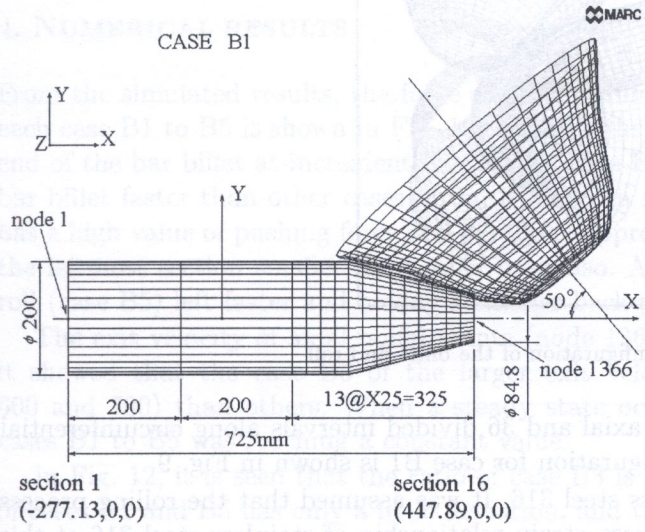

Fig. 5. Deformable bar billet for case B1

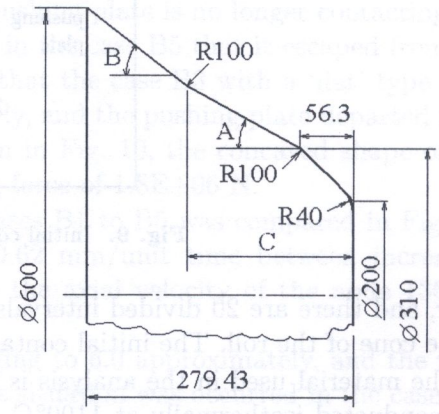

Fig. 6. Dimensions of roll for cases B1 to B5

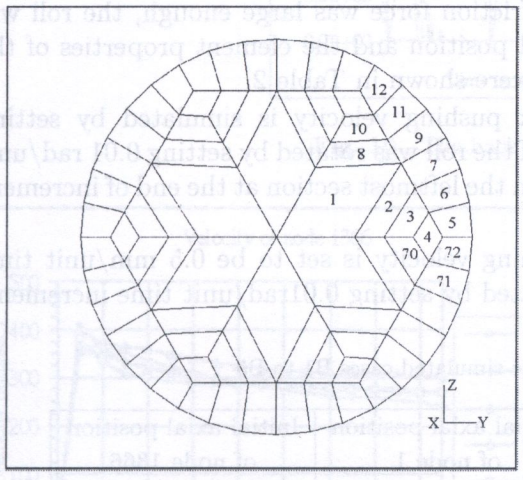

Fig. 7. Numbering system of elements

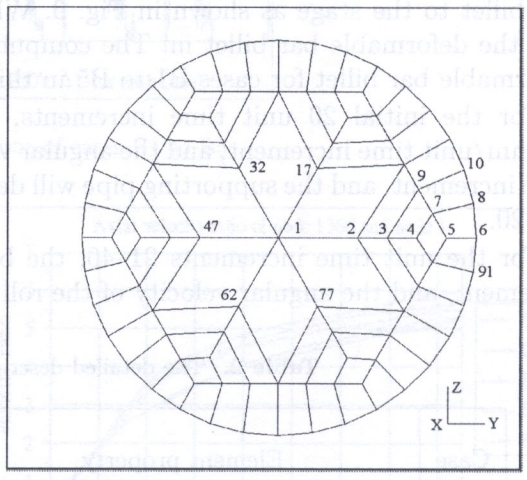

Fig. 8. Numbering system of nodes

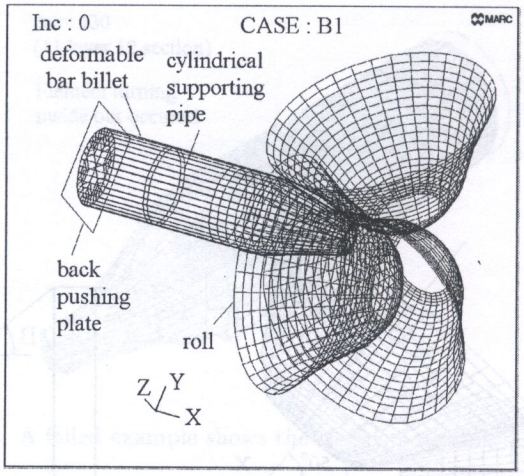

Fig. 9. Initial contact configuration of the billet and roll

body, and there are 20 divided intervals along axial and 36 divided intervals along circumferential of the cone of the roll. The initial contact configuration for case B1 is shown in Fig. 9.

The material used in the analysis is stainless steel 316. It was assumed that the rolling process was conducted isothermally at 1100°C. The stress–strain relationship of stainless steel 316 at this temperature is obtained by compressing test and modeled by a bilinear function.

The material property are described in detail as follows: The strain hardening rate (H) is 116 MPa when $\varepsilon < 0.50$ and 10 MPa when $\varepsilon \geq 0.50$; the Young's modulus (E) is 79 MPa, the yielding stress is 100 MPa, and Poisson's ratio is 0.33. The coefficient of friction is set to be 0.5 to correspond the hot-working processes. The offset angle (α) and inclined angle (β) of the rolls are set to be 7° and 50°, respectively.

Every three-dimensional brick element bears a twenty-four degrees of freedom and three-degrees of freedom per node. Because of the different roll's shape, the initial contact position between the billet and the rolls are different and it can be found by using a self-written Fortran program to compute the right configuration. The initial contact configuration of the billet and rolls can be found by the method of halving the interval (bisection method). It was necessary to push the deformable bar billet to the stage as shown in Fig. 9. When the friction force was large enough, the roll will pull the deformable bar billet in. The computed initial position and the element properties of the deformable bar billet for cases B1 to B5 in this study were shown in Table 2.

For the initial 20 unit time increments, the back pushing velocity is simulated by setting 1.0 mm/unit time increment, and the angular velocity of the roll was rotated by setting 0.01 rad/unit time increment, and the supporting pipe will depart from the leftmost section at the end of increment No. 20.

For the unit time increments 21–40, the back pushing velocity is set to be 0.5 mm/unit time increment, and the angular velocity of the roll was rotated by setting 0.01rad/unit time increment.

Table 2. The detailed description of the simulated cases B1 to B5

Case	Element property	Initial axial position of node 1 on section 1 mm	Initial axial position of node 1366 on section 16 mm
B1	Node= 1456 Element = 1080 Section= 16 Degree of freedom of the billet = 4368	−277.13	447.89
B2		−279.58	445.42
B3		−283.21	441.79
B4		−296.09	428.91
B5		−315.58	409.42

For the unit time increments 41–60, the back pushing velocity is set to be 0.25 mm/unit time increment, and the angular velocity of the roll was rotated by setting 0.01 rad/unit time increment.

After 60 unit time increments, the process proceeds by rotating the rolls only.

4. Numerical results

From the simulated results, the force of back pushing plate from initial state to increment 250 for each case B1 to B5 is shown in Fig. 10. From it, the back pushing plate is no longer contacting the end of the bar billet at increment No. 125 for case B1. But in the case B5 that it escaped from the bar billet faster than other cases. From it, one can realize that the case B3 with a 'flat' type cone has a high value of pushing force of 3.0E+06 N approximately, and the pushing plate departed from the leftmost section smaller than other case also. As shown in Fig. 10, the concaved shape of the roll (case B5) left faster and having a smaller back pushing force of 1.8E+06 N.

The exit velocity of axial nodal points (node 1366) of cases B1 to B5 was compared in Fig. 11, it showed that the case B3 of the larger exit velocity (0.62 mm/unit time between increment 600 and 700) than others. When a steady state occurred, the axial velocity of the node 1366 of cases B1 to B5 was reaching a constant value.

In Fig. 12, it is seen that the ratio of case B3 is converging to 6.0 approximately, and the ratio of cases B1 and B5 has only a little deviation, and the same situation was occurred in the cases B2

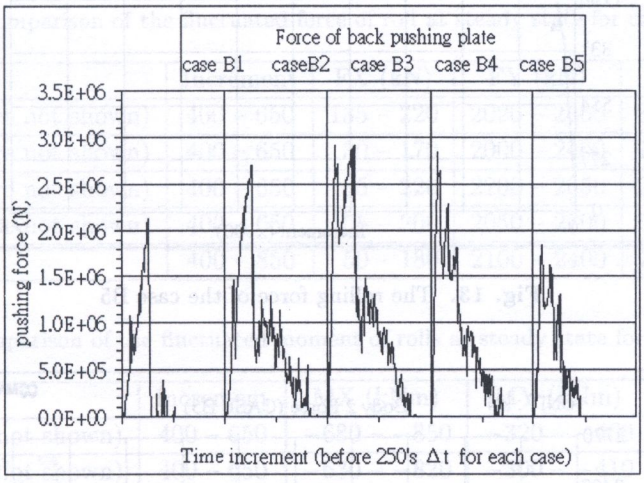

Fig. 10. The back pushing force of cases B1 to B5

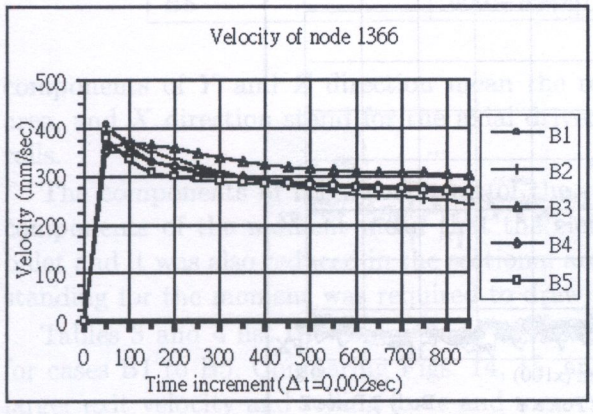

Fig. 11. The exit velocity of node 1366 for cases B1 to B5

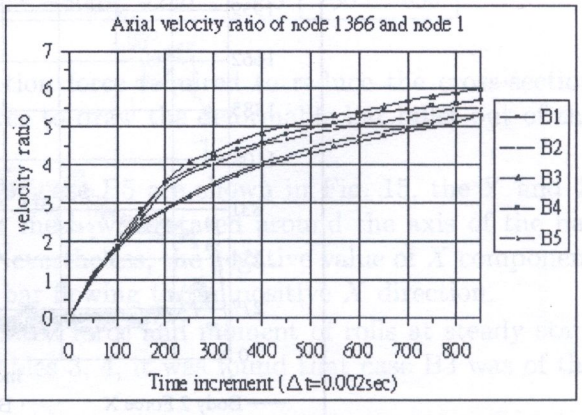

Fig. 12. Axial velocity ratio of cases B1 to B5

and B4. Owing to the initial push of the back pushing plate (a total of 35 mm axial displacement), the velocity increment before increment No. 400 had a higher value.

The total rolling force of the case B5 is shown in Fig. 13. It can be easily determined by checking that the fluctuated rolling force of roll is circulating between increment No. 400 and No. 850. It seems that the deformation reached steady state between increment No. 400 and 800, and it became non-steady beyond the increment 850 because the inlet element mesh was very large and was still in elastic state. Note that the rolling force fluctuated in the process because some of the circumferential nodes are in contact with and/or depart from the rolls. In Fig. 14, the rolling force

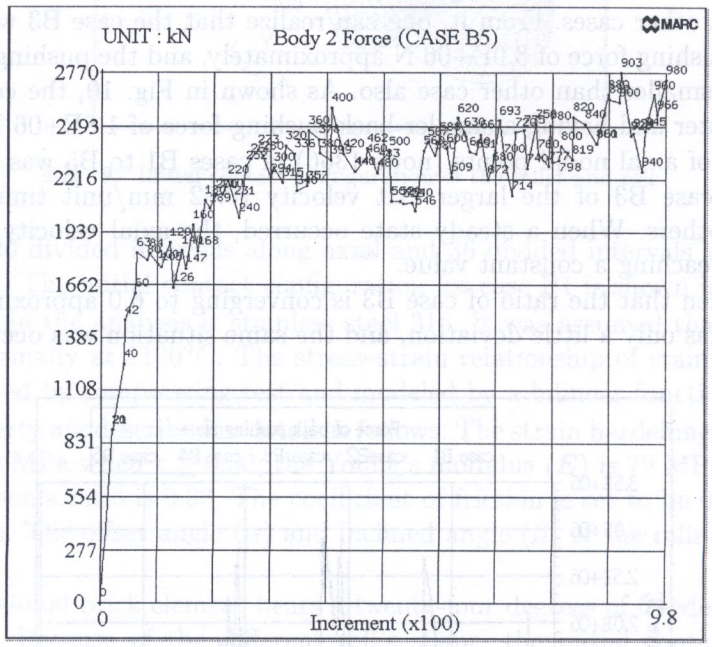

Fig. 13. The rolling force of the case B5

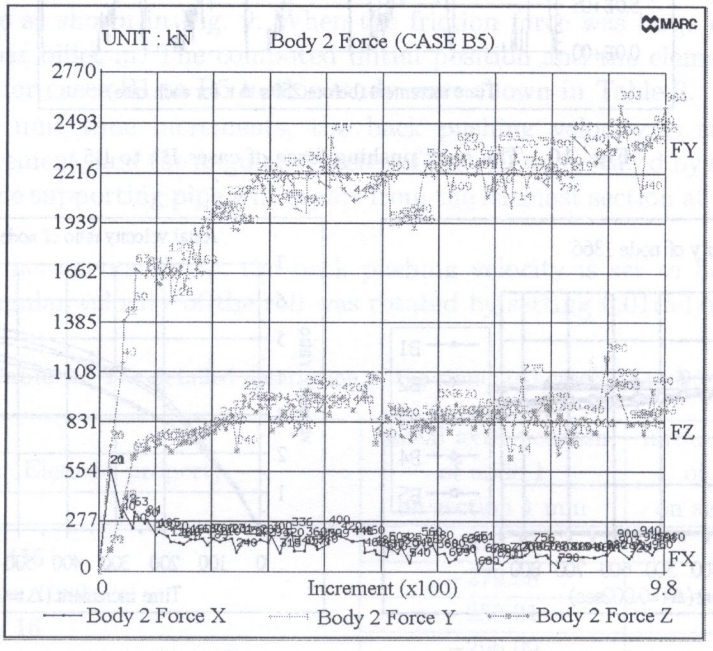

Fig. 14. The rolling force components of the case B5

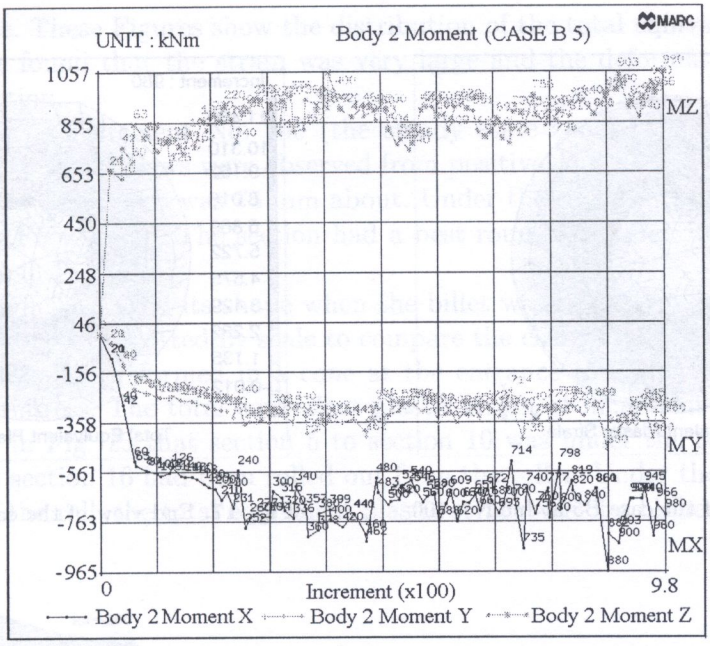

Fig. 15. The rolling moment components of the case B5

Table 3. Comparison of the fluctuated force of roll at steady state for cases B1 to B5

Case	Increment	FX (kN)	FY (kN)	FZ (kN)
B1 (figure not shown)	400 – 650	135 – 220	2020 – 2560	800 – 1100
B2 (figure not shown)	400 – 650	30 – 170	2000 – 2400	760 – 1000
B3 (figure not shown)	400 – 650	65 – 220	2200 – 2650	900 – 1150
B4 (figure not shown)	400 – 650	55 – 200	2050 – 2700	825 – 1150
B5	400 – 850	50 – 180	2100 – 2400	700 – 1050

Table 4. Comparison of the fluctuated moment of rolls at steady state for cases B1 to B5

Case	Increment	MX (kNm)	MY (kNm)	MZ (kNm)
B1 (figure not shown)	400 – 650	−680 – −850	−320 – −460	850 – 1150
B2 (figure not shown)	400 – 650	−630 – −820	−300 – −410	800 – 1080
B3 (figure not shown)	400 – 650	−680 – −900	−330 – −410	925 – 1200
B4 (figure not shown)	400 – 650	−680 – −920	−330 – −450	810 – 1220
B5	400 – 850	−600 – −800	−250 – −360	750 – 950

components of Y and Z direction mean the reduction force required to reduce the cross-section area, and X direction stand for the axial driven force to draw the deformable bar billet out of the rolls.

The components of rolling moment of the roll for case B5 are shown in Fig. 15, the Y and Z components of the moment mean that the element mesh was rotated around the axis of the bar billet and it was also reduced in the sectional area. Nevertheless, the negative value of X component standing for the moment was required to draw the bar flowing to the positive X direction.

Tables 3 and 4 list the components of the fluctuated force and moment of rolls at steady state for cases B1 to B5. Comparing Figs. 14, 15, and Tables 3, 4, it was found that case B3 was of the larger exit velocity and rolling force and moment.

The end views of the billet for case B5 at the increments No. 700 and No. 980 were shown in Figs. 16 and 17, respectively. It was cleared that the elements were rotated in a direction of

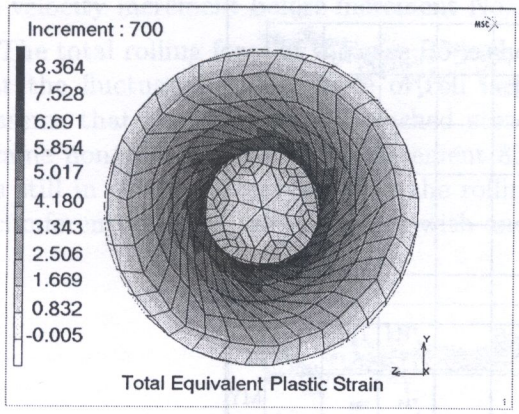

Fig. 16. End view of the case B5 at Inc No. 700

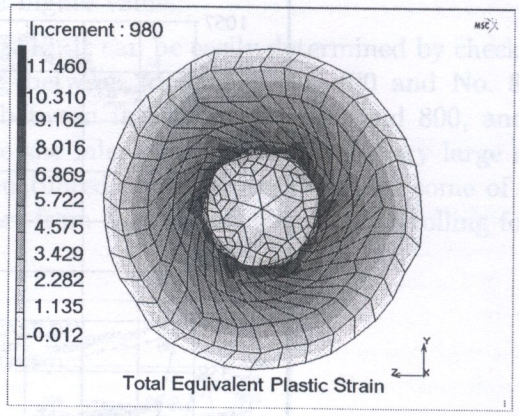

Fig. 17. End view of the case B5 at Inc No. 980

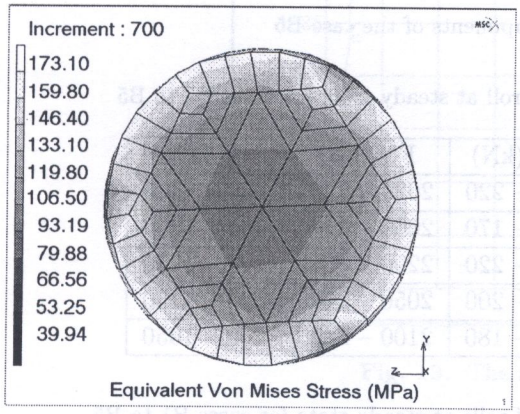

Fig. 18. Sectional view of section 6 for case B5

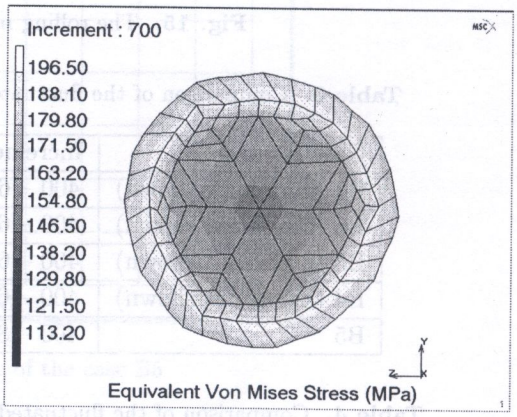

Fig. 19. Sectional view of section 8 for case B5

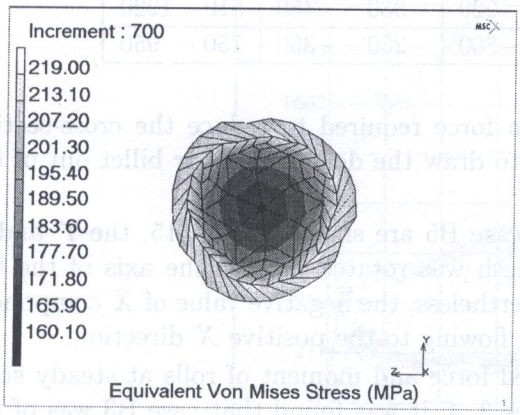

Fig. 20. Sectional view of section 10 for case B5

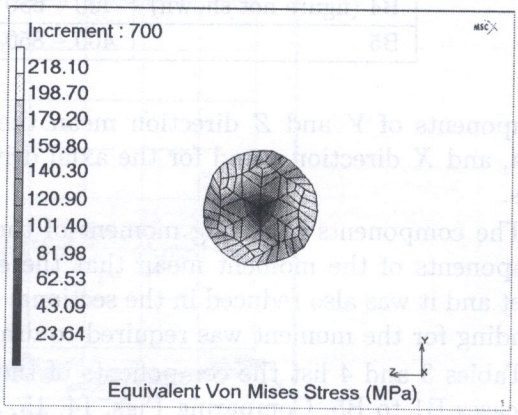

Fig. 21. Sectional view of section 14 for case B5

clockwise along X-axis. These Figures show the distribution of the total equivalent plastic strain of the element, it can be found that the strain was very large and the deformation was also of very large with a huge rotation.

The sectional views at increment No. 700 (the steady state zone) of the billet are shown in Figs. 18–21, all of the sectional views were observed from positive X direction. The entrance size of the billet was 200 mm and the exit was 75 mm about. Under the roll gap the section of the billets were oval as shown in Figs. 18–20. The section had a best roundness when it had been rolled out from the roll as shown in Fig. 21.

The profile of the billet changed its shape when the billet was rolled out. In Fig. 22, the profile from increment 200 to 980 was plotted by scale to compare the changes at the correspondent stage.

Because of the billet was preformed in a cone at the entrance that the exit sectional element had a various value of stress. The total equivalent plastic strain at increment No. 980 is shown in Fig. 23. It was found in Fig. 23 that section 5 to section 10 was under the reduction zone of the roll, but section 11 to section 16 had been rolled out from the roller. Under the reduction zone and after the exit plane of the roll, the total equivalent plastic strain was of a higher value (about 11.46) than other zone.

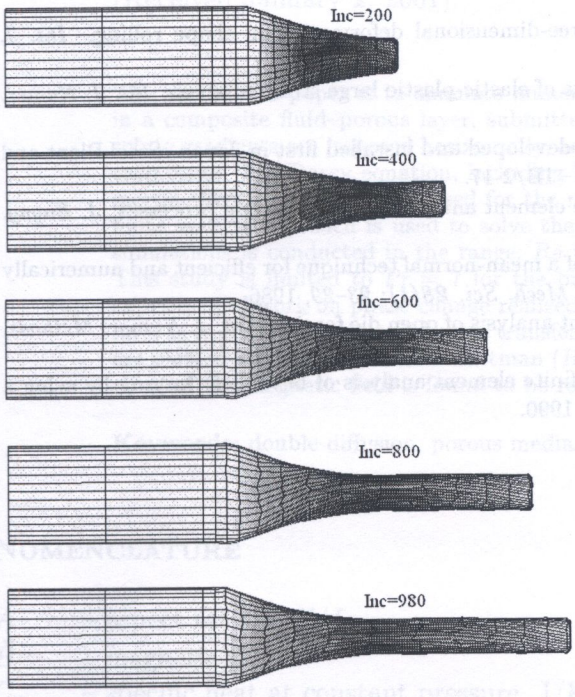

Fig. 22. The profile change of the billet for case B5

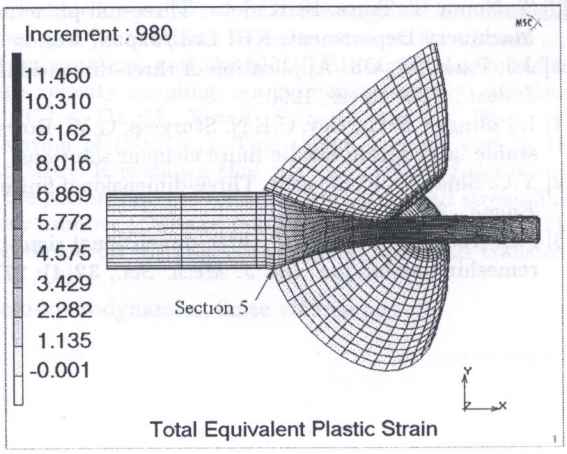

Fig. 23. The distribution of the total equivalent plastic strain for case B5

5. Conclusion

This present research shows the possibility of the simulation of three-roll planetary mill by a various shapes of roll. The total computation required on a CONVEX C3840 for any one case of cases B1 to B5 with 1000 increment was 3000 CPU minutes about. It is suggested that the circumferential nodal point and the elements of the subdivided billet should posses a symmetrical relation with the numbers of roll. In order to overcome the element turning inside out, a rezoning procedure should be adopted. Comparing the computed moments and the flow speeds of the billet, it is suggested that the "flat" type cone of the roll (case B3) has a good results in increasing output than the others. From the computed values, the moment of the roll can be used to develop a new product

by estimating the consuming power of the roll system, and the rolling force is a useful data for designing the bearing system of the three-roll planetary mill, and the computed exit velocity of the billet can be used to predict the output of the plant. So, the simulation results of this research can take a prediction of the practice of the rolling process.

REFERENCES

[1] W.J. Ammerling et al. The knocks 3-roll technology for high precision specialty rod and bar products. *MPT-Metallurgical Plant and Technology*, **6**: 14–19, 1989.

[2] K. Aoyagi, K. Ohta. Material deformation, rolling load and torque in 3-roll planetary mill. *J. Japan Plasticity and Machining*, **24**: 1039–1047, 1983.

[3] H.D. Hibbitt, P.V. Marcal, J.R. Rice. A finite element formulation for problems of large strain and large displacement. *Int. J. Solids Structures*, **6**: 1069–1086, 1970.

[4] Ir A.W.A. Konter. Special topic course on metal forming analysis using the finite element methods. MARC Analysis Research Corporation – Europe, Zoetermeer, October 15–16, 1987.

[5] G.-J. Li, S. Kobayashi. Rigid plastic finite-element analysis of plane strain rolling. *Journal of Engineering for Industry*, **104**: 55–64, 1982.

[6] R.M. McMeeking, J.R. Rice. Finite-element formulations for problems of large elastic-plastic deformation. *Int. J. Solids Structures*, **11**: 601–616, 1975.

[7] K. Mori, K. Osakada. Finite element simulation of three-dimensional deformation in shape rolling. *Int. J. Numer. Methods Engng.*, **30**: 1431–1440, 1990.

[8] J.C. Nagtegaal, J.E. de Jong. Some computational aspects of elastic-plastic large strain analysis. *Int. J. Numer. Methods. Engng.*, **17**: 15–41, 1981.

[9] T. Noma, T. Tsuta, K. Kadota. Three-roll planetary mill developed and installed first in Japan. Steel Plant and Machinery Department, KHI Ltd./Japan, session 1B/2-0 – 1B/2-17.

[10] J.J. Park, S.I. Oh. Application of three-dimensional finite element analysis to shape rolling processes, *J. Engng. Indust.*, **112**: 36–46, 1990.

[11] I. Pillinger, P. Hartley, C.E.N. Sturgess, G.W. Rowe. Use of a mean-normal technique for efficient and numerically stable large-strain elastic finite element solutions. *Int. J. Mech. Sci. 28(1): 23–29*, 1986.

[12] Y.C. Shiau, S. Kobayashi. Three-dimensional finite element analysis of open die forging. *Int. J. Numer. Methods. Engng.*, **25**: 67–85, 1988.

[13] J.H. Yoon, D.Y. Yang. A three-dimensional rigid-plastic finite element analysis of bevel gear forging by using a remeshing technique. *Int. J. Mech. Sci.*, **32**(4): 277–291, 1990.